involve
a journal of mathematics

Global sensitivity analysis in a mathematical model of the renal insterstitium

Mariel Bedell, Claire Yilin Lin,
Emmie Román-Meléndez and Ioannis Sgouralis

msp

2017 vol. 10, no. 4

INVOLVE 10:4 (2017)
dx.doi.org/10.2140/involve.2017.10.625

Global sensitivity analysis in a mathematical model of the renal insterstitium

Mariel Bedell, Claire Yilin Lin,
Emmie Román-Meléndez and Ioannis Sgouralis

(Communicated by Suzanne Lenhart)

The pressure in the renal interstitium is an important factor for normal kidney function. Here we develop a computational model of the rat kidney and use it to investigate the relationship between arterial blood pressure and interstitial fluid pressure. In addition, we investigate how tissue flexibility influences this relationship. Due to the complexity of the model, the large number of parameters, and the inherent uncertainty of the experimental data, we utilize Monte Carlo sampling to study the model's behavior under a wide range of parameter values and to compute first- and total-order sensitivity indices. Characteristically, at elevated arterial blood pressure, the model predicts cases with increased or reduced interstitial pressure. The transition between the two cases is controlled mostly by the compliance of the blood vessels located before the afferent arterioles.

1. Introduction

Kidneys are the core organs in the urinary system. Their principal functions are to remove metabolic waste from the blood and to regulate blood salt and water levels [Eaton et al. 2009]. Through the regulation of salt and water, kidneys also play an important role in the regulation of arterial blood pressure [Cowley 1997; Wolgast et al. 1981]. To perform these functions, each kidney adjusts the composition of the urine it produces.

Each kidney has an outer layer, called the *cortex*, and an inner layer, known as the *medulla* [Kriz and Bankir 1988]. Much of the space in these regions is filled by the functional units of the kidney, which are termed *nephrons*. Depending on the organism, each kidney contains thousands to millions of nephrons. Nephrons are responsible for the production of urine.

Kidneys contain two types of nephrons, cortical (short) and juxtamedullary (long) nephrons, each of which is surrounded by a net of capillaries. Cortical

MSC2010: primary 49Q12, 65C05, 92C30, 93A30; secondary 92C50, 92C42.
Keywords: mathematical model, sensitivity analysis, Monte Carlo, kidney, interstitium.

nephrons remain almost entirely in the cortex, while juxtamedullary nephrons extend deep into the medulla. Each nephron consists of a *glomerulus* and a *renal tubule*. Furthermore, each renal tubule consists of various permeable or impermeable segments [Eaton et al. 2009; Kriz and Bankir 1988]. Additionally, each nephron has access to a collecting duct for removal of the produced urine.

Kidneys are connected with the rest of the body by two blood vessels, the renal artery, which carries blood into the kidney, and the renal vein, which carries blood out of the kidney to recirculate into the body. In addition, urine is excreted from the body through the ureter. Blood coming from the renal artery is delivered to the afferent arterioles. A steady flow of blood coming from the afferent arteriole of a nephron is filtered in the glomerulus and flows into the renal tubule. The blood flow is maintained constant in each glomerulus by the constriction or relaxation of its afferent arteriole [Holstein-Rathlou and Marsh 1994; Sgouralis and Layton 2015]. Nearly all of the fluid that passes through the renal tubules is reabsorbed and only a minor fraction results in urine. Fluid is reabsorbed from the renal tubules in two stages: first by the renal interstitium and then by the surrounding capillaries. The processes underlying reabsorption are driven by the pressures in the interstitial spaces [Cowley 1997; Wolgast et al. 1981].

The pressures in the renal interstitium are important determinants of kidney function. There is a lack of investigations that look at the factors affecting them. We develop a computational model of the rat kidney, for which several experimental data exist, and use it to study the relationship between arterial blood pressure and interstitial fluid pressure. In addition, we study how tissue flexibility affects this relationship and how the model predictions are affected by the uncertainty of key model parameters. We model the uncertain parameters as random variables and quantify their impact using Monte Carlo sampling and global sensitivity analysis.

2. Methods

2.1. ***Model description.*** The model consists of a collection of compartments that follow the characteristic anatomy of the kidneys of mammals [Kriz and Bankir 1988; Moffat and Fourman 1963]. The compartments fall in three categories:

(i) *regions* that model the cortical and medullary interstitial spaces,

(ii) *pipes* that model the blood vessels and renal tubules, and

(iii) *spheres* that model the glomeruli.

A schematic diagram depicting the arrangement of the compartments (1–35) is shown in Figure 1 and a summary is given in Table 1. To facilitate the description of the model equations below, we use a set of nodes (c1–c32) to mark the connections of the compartments; these nodes are also included in Figure 1 and Table 1.

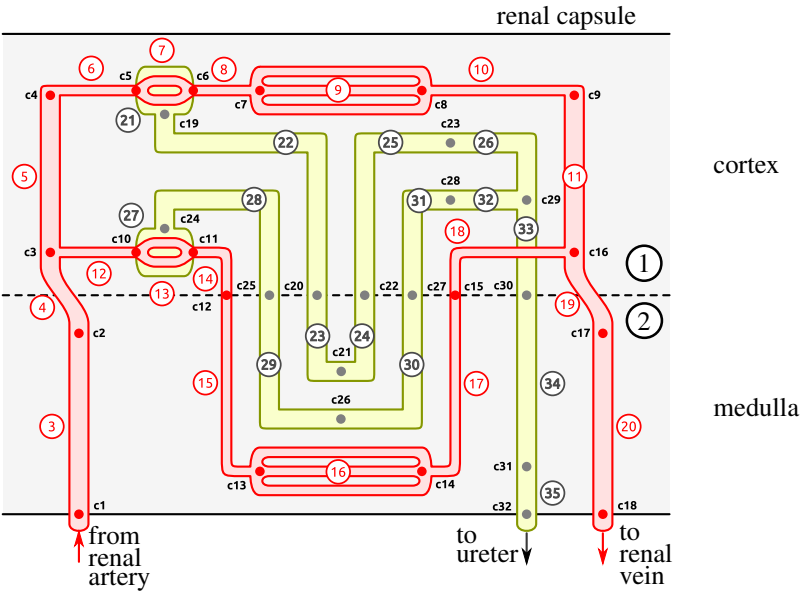


Figure 1. Schematic diagram of the model kidney. It shows the arrangement of blood vessels (red) and nephrons (yellow) within the interstitial spaces (gray). With the exceptions of the capillaries, the schematic displays only one of each of the different compartments contained in the full model. Nodes c1–c32 mark the connections of the compartments.

Briefly described, blood enters through the renal artery (node c1) and splits into a number of large arteries (compartments 3–5) that drain to the afferent arterioles (compartments 6 and 12). Each afferent arteriole supplies one glomerulus (compartments 21 and 27). In the glomeruli, blood is divided between the efferent arterioles (compartments 8 and 14) and the renal tubules (compartments 22–26 and 28–32). Leaving the efferent arterioles, blood passes through the cortical microcirculation (compartments 9 and 10) or the medullary microcirculation (compartments 15–18), before it rejoins in large veins (compartments 11, 19, and 20) and leaves through the renal vein (node c18).

The model represents short (compartments 21–26) and long nephrons (compartments 27–32) that both drain in the same collecting duct (compartments 33–35), which, in turn, drains to the ureter (node c32). The model accounts for the spacial as well as the anatomical differences between the two nephrons that are developed in the mammalian kidney [Kriz and Bankir 1988; Moffat and Fourman 1963]. For example, the model accounts for differences in the location within the cortex or medulla, in the pre- and postglomerular vascular supply, dimensions, reabsorptive capacity, etc.

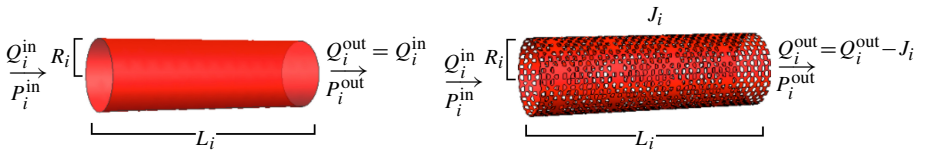


Figure 2. Model pipes: impermeable pipe, left, and permeable pipe, right.

2.1.1. *Model pipes and spheres.* Blood vessels and renal tubules are modeled as distensible pipes, while glomeruli are modeled as distensible spheres. Fluid flows through a compartment i at a volumetric rate of Q_i (Figure 2). Following the physiology, some of the pipes are considered permeable while others are impermeable [Eaton et al. 2009]. For simplicity, we assume that the only pipes modeling blood vessels that are permeable are those that model capillaries.

The flow that passes through the walls of a permeable pipe is denoted by J_i. According to the common convention, $J_i > 0$ denotes fluid leaving the pipe and $J_i < 0$ denotes fluid entering the pipe. Due to conservation of mass, the flow that leaves from an impermeable pipe Q_i^{out} is the same as the flow that enters Q_i^{in}, thus

$$Q_i^{\text{out}} = Q_i^{\text{in}}, \tag{1}$$

while the flow that leaves a permeable pipe is given by

$$Q_i^{\text{out}} = Q_i^{\text{in}} - J_i. \tag{2}$$

We assume that the flow crossing through the walls of renal tubules and glomerular capillaries is a constant fraction of the corresponding inflow

$$J_i = f_i Q_i^{\text{in}}, \tag{3}$$

where f_i is the fraction of fluid that crosses through the pipe's wall. For the coefficients f_i we use the values listed in Table 1, which are chosen such that the model predicts flows similar to the antidiuretic rat model in [Moss and Layton 2014].

Flows through the walls of the cortical and medullary capillaries are computed by the Starling equation [Wolgast et al. 1981]:

$$J_9 = K_f^9(P_9 - P_1 + \pi_9 - \pi_1), \tag{4}$$

$$J_{16} = K_f^{16}(P_{16} - P_2 + \pi_{16} - \pi_2), \tag{5}$$

where $K_f^9 = 1.59\,\mu\text{m}^3/\text{mmHg/min}$ and $K_f^{16} = 2.28\,\mu\text{m}^3/\text{mmHg/min}$ are the filtration coefficients of the cortical and medullary capillaries and π_1, π_2, π_9, and π_{16} are the oncotic pressures and P_1, P_2, P_9, and P_{15} are the hydrostatic pressures in the

i	compartment (type)	number	P_i^{int}	P_i^{ext}	nodes	frac. coeff.
1	Cortical interstitium (region)	1	P_1	-	-	-
2	Medullary interstitium (region)	1	P_2	-	-	-
3	Medullary artery (pipe)	8	P_3	P_2	c1–c2	0
4	Arcuate artery (pipe)	24	P_4	$\frac{1}{2}(P_1 + P_2)$	c2–c3	0
5	Cortical radial artery (pipe)	864	P_5	P_1	c3–c4	0
6	Afferent arteriole$^{\text{sn}}$ (pipe)	20736	P_6	P_1	c4–c5	0
7	Glomerular capillary$^{\text{sn}}$ (pipe)	5598720	P_7	P_{c19}	c5–c6	$3/28$
8	Efferent arteriole$^{\text{sn}}$ (pipe)	20736	P_8	P_1	c6–c7	0
9	Cortical capillary (pipe)	1658880	P_9	P_1	c7–c8	see (4)
10	Venule$^{\text{sn}}$ (pipe)	20736	P_{10}	P_1	c8–c9	0
11	Cortical radial vein (pipe)	864	P_{10}	P_1	c9–c16	0
12	Afferent arteriole$^{\text{ln}}$ (pipe)	10368	P_{12}	P_1	c3–c10	0
13	Glomerular capillary$^{\text{ln}}$ (pipe)	4302720	P_{13}	P_{c24}	c10–c11	$3/28$
14	Efferent arteriole$^{\text{ln}}$ (pipe)	10368	P_{14}	P_1	c11–c12	0
15	Descending vas rectum (pipe)	207360	P_{15}	P_2	c12–c13	0
16	Medullary capillary (pipe)	10368000	P_{16}	P_2	c13–c14	see (5)
17	Ascending vas rectum (pipe)	414720	P_{17}	P_2	c14–c15	0
18	Venule$^{\text{sn}}$ (pipe)	10368	P_{18}	P_1	c15–c16	0
19	Arcuate vein (pipe)	24	P_{19}	$\frac{1}{2}(P_1 + P_2)$	c16–c17	0
20	Medullary vein (pipe)	8	P_{20}	P_2	c17–c18	0
21	Glomerulus$^{\text{sn}}$ (sphere)	20736	P_{c19}	P_1	c19	–
22	Proximal tubule$^{\text{sn}}$ (pipe)	20736	P_{22}	P_1	c19–c20	$2/3$
23	Descending limb$^{\text{sn}}$ (pipe)	20736	P_{23}	P_2	c20–c21	$3/10$
24	Medullary ascending limb$^{\text{sn}}$ (pipe)	20736	P_{24}	P_2	c21–c22	0
25	Cortical ascending limb$^{\text{sn}}$ (pipe)	20736	P_{c24}	P_1	c22–c23	0
26	Distal tubule$^{\text{sn}}$ (pipe)	20736	P_{26}	P_1	c23–c29	$13/84$
27	Glomerulus$^{\text{ln}}$ (sphere)	10368	P_{24}	P_1	c24	–
28	Proximal tubule$^{\text{ln}}$ (pipe)	10368	P_{28}	P_1	c24–c25	$2/3$
29	Descending limb$^{\text{ln}}$ (pipe)	10368	P_{29}	P_2	c25–c26	$5/12$
30	Medullary ascending limb$^{\text{ln}}$ (pipe)	10368	P_{30}	P_2	c26–c27	0
31	Cortical ascending limb$^{\text{ln}}$ (pipe)	10368	P_{31}	P_1	c27–c28	0
32	Distal tubule$^{\text{ln}}$ (pipe)	10368	P_{32}	P_1	c28–c29	0
33	Cortical collecting duct (pipe)	144	P_{33}	P_1	c29–c30	$13/84$
34	Medullary collecting duct (pipe)	144	P_{34}	P_2	c30–c31	$12/13$
35	Papillary collecting duct (pipe)	8	P_{35}	P_2	c31–c32	0

Table 1. Summary of the compartments contained in the kidney model. Superscripts sn and ln denote short and long nephrons, respectively. Number refers to the total number of compartments contained in the full model.

associated compartments. The oncotic pressures are obtained by an approximation of the Landis–Pappenheimer relation

$$\pi_i = \alpha C_i + \beta C_i^2, \tag{6}$$

where $\alpha = 1.63\,\text{mmHg}\cdot\text{dl/gr}$ and $\beta = 0.29\,\text{mmHg}\cdot\text{dl}^2/\text{gr}^2$ as used in [Deen et al. 1972]. In (6), C_i denotes the concentration of protein in the compartment i. We assume a fixed protein concentration of the blood entering through the renal artery of $C_a = 5.5\,\text{gr/dl}$ and compute concentrations throughout the blood vessels (compartments 3–9 and 12–16) by taking into consideration conservation of mass:

$$C_i^{\text{out}} = \frac{Q_i^{\text{in}}}{Q_i^{\text{in}} - J_i} C_i^{\text{in}}, \tag{7}$$

where C_i^{in} and C_i^{out} denote the inflow and outflow concentrations of the compartment i. The oncotic pressures π_9 and π_{16} in (4) and (5) are computed based on the averages

$$C_9 = \tfrac{1}{2}(C_9^{\text{in}} + C_9^{\text{out}}), \tag{8}$$

$$C_{16} = \tfrac{1}{2}(C_{19}^{\text{in}} + C_{19}^{\text{out}}). \tag{9}$$

In each pipe and glomerulus, the internal pressure is denoted P_i^{int} and the external P_i^{ext}. For pipes, P_i^{int} is computed by the average of the pressures at the associated inflow and outflow nodes (Figure 1). For the glomeruli, internal pressure equals to the pressure of the associated node (Figure 1 and Table 1). For all pipes and glomerulus compartments, the external pressures equal the internal pressure of the surrounding compartment, which, in the case of the cortical and medullary regions, are denoted by P_1 and P_2, respectively. Exceptions to this are the arcuate arteries and veins (compartments 4 and 19, respectively), which anatomically are located between the cortex and the medulla [Kriz and Bankir 1988], so we compute P_i^{ext} for these compartments by the average of P_1 and P_2.

The volumes of the compartments, besides the regions and the afferent arterioles (compartments 1, 2, 6, and 12), depend *passively* on the pressure difference that is developed across their walls:

$$V_i = V_i^{\text{ref}} + s_i(P_i^{\text{int}} - P_i^{\text{ext}} + \Delta P_i^{\text{ref}}), \tag{10}$$

where V_i^{ref}, ΔP_i^{ref}, and s_i are constants. In particular, V_i^{ref} and ΔP_i^{ref} denote a reference volume and the pressure difference across the walls of the compartment when V_i equals V_i^{ref}, respectively. The parameters s_i are a measure of the distensibility of the compartments. A large s_i value indicates a compartment that is very distensible, while a low value s_i indicates a more rigid compartment. In the

model, we use $s_i \geq 0$ such that an increase in P_i^{int} or a decrease in P_i^{ext} leads to an expansion of the volume V_i, and vice versa.

For a model pipe, let P_i^{in} and P_i^{out} denote the pressures at its inflow and outflow nodes, respectively. These pressures are related by a modified form of the Poiseuille law:

$$P_i^{\text{in}} - P_i^{\text{out}} = \frac{8\mu_i L_i}{\pi R_i^4}\left(Q_i^{\text{in}} - \tfrac{2}{3}J_i\right), \tag{11}$$

where μ_i is the viscosity of the flowing fluid, L_i is the length of the pipe, and R_i is its radius. In the model, we assume μ_i and L_i to be constants, while we compute R_i based on the compartment's volume (i.e., $V_i = \pi R_i^2 L_i$). Equation (11) reduces to the common Poiseuille equation for the impermeable pipes [Sgouralis and Layton 2015], while for the permeable pipes, it is assumed that J_i is linearly distributed along the length of the pipe with a value of zero at the end of the pipe.

Pressure at node c1 equals the arterial blood pressure P_a, which in our model is a free variable. Pressures at nodes c18 and c32 are kept constant at 4 mmHg and 2 mmHg, respectively, in agreement with the values of venous and ureter pressures used in previous modeling studies [Moss and Thomas 2014; Layton et al. 2012].

2.1.2. *Model afferent arterioles.* The afferent arterioles are unique vessels in the sense that they *actively* adjust radii such that blood flows through them at a fixed rate [Holstein-Rathlou and Marsh 1994; Sgouralis and Layton 2015]. In the model, we assume that blood flows in the afferent arterioles that feed the short and long nephrons (i.e., Q_6 and Q_{12}, respectively) are fixed at 280 nl/min and 336 nl/min, respectively, as in previous modeling studies of renal hemodynamics (see, for example, [Moss and Layton 2014; Fry et al. 2014; Sgouralis and Layton 2014]).

We compute the radii of the afferent arterioles by using the Poiseuille equation [Sgouralis and Layton 2015], which yields

$$R_6 = \left(\frac{8\mu_6 L_6}{\pi}\frac{Q_6}{P_{c4} - P_{c5}}\right)^{1/4}, \tag{12}$$

$$R_{12} = \left(\frac{8\mu_{12} L_{12}}{\pi}\frac{Q_{12}}{P_{c3} - P_{c10}}\right)^{1/4}. \tag{13}$$

Note that (12) and (13) imply that whenever the pressure difference along the afferent arterioles $P_{c4} - P_{c5}$ and $P_{c3} - P_{c10}$ increases, the radii R_6 and R_{12} decrease. This, in turn, implies that whenever the arterial blood pressure P_a increases, the afferent arterioles constrict, and thus the total volumes occupied by them, $V_6 = \pi R_6^2 L_6$ and $V_{12} = \pi R_{12}^2 L_{12}$, are reduced.

2.1.3. *Model interstitial regions.* The cortical and medullary interstitial spaces, i.e., compartments 1 and 2, lie outside of the compartments 3–35 and therefore must be calculated separately using a different set of equations. We obtain the first

of such relationships by assuming that the net accumulation of interstitial fluid within the cortex and medulla is zero. That is,

$$J_9 + \tfrac{1}{80} J_{22} + \tfrac{1}{80} J_{26} + \tfrac{1}{160} J_{28} + \tfrac{1}{160} J_{32} = 0, \tag{14}$$

$$J_{16} + \tfrac{1}{500} J_{23} + \tfrac{1}{1000} J_{29} + \tfrac{1}{72000} J_{34} = 0, \tag{15}$$

where the flows J_i are weighted based on the total number of the compartments contained in the full model (Table 1).

Equations (4) and (5) require the oncotic pressures π_1 and π_2, which in turn require the cortical and medullary protein concentrations C_1 and C_2 for (6). Protein concentrations in the cortical and medullary regions are computed assuming that the total mass of protein contained in each region, M_1 and M_2, respectively, remains constant. Thus,

$$C_1 = M_1/V_1, \tag{16}$$

$$C_2 = M_2/V_2. \tag{17}$$

We use the values $M_1 = 1.93$ mgr and $M_2 = 1.25$ mgr, which are computed such that the resulting model predicts reference pressures in the renal cortex and medulla of ~ 6 mmHg, similar to those estimated experimentally [Cowley 1997].

Cortical and medullary interstitial volumes V_1 and V_2 are assumed to change proportionally; thus,

$$V_1/V_2 = \kappa, \tag{18}$$

where κ is the proportionality constant. The combined volume of the interstitial regions V_1+V_2 is calculated based on the total volume of the kidney V_0 according to

$$V_1 + V_2 = V_0 - V_{\text{cortex}} - V_{\text{medulla}}, \tag{19}$$

where V_{cortex} and V_{medulla} are found by summing the total volumes of the pipe and glomerulus compartments contained within each region. Finally, the total volume of the kidney V_0 is calculated by

$$V_0 = V_0^{\text{ref}} + s_0\,(P_1 - P_0^{\text{ext}} + \Delta P_0^{\text{ref}}), \tag{20}$$

where in this case P_0^{ext} refers to the pressure external to the kidney, which is set to 0 mmHg. Equation (20) assumes that the total volume of the kidney is determined by the distensibility of the renal capsule s_0, which is stretched by the difference of the pressures developed across it, i.e., $P_1 - P_0^{\text{ext}}$.

2.2. ***Model parameters.*** Values for the model parameters are given in Table 2. These values are chosen such that at a reference arterial blood pressure $P_a^{\text{ref}} = 100$ mmHg, the model predicts pressures and volumes that are in good agreement

i	L_i μm	μ_i	P_i^{ref} mmHg	ΔP_i^{ref} mmHg	R_i^{ref} μm	V_i^{ref} μm^3	$\tilde{\sigma}_i$	ci	$P_{\text{ci}}^{\text{ref}}$ mmHg
1	-	-	6	-	-	$7.62 \cdot 10^{10}$	-	c1	100
2	-	-	6	-	-	$4.92 \cdot 10^{10}$	-	c2	97.51
3	$7 \cdot 10^3$	μ_L	98.75	−92.75	270	$1.60 \cdot 10^9$	$\tilde{\sigma}_{G4}$	c3	95.02
4	$2 \cdot 10^3$	μ_L	96.26	−90.26	150	$1.41 \cdot 10^8$	$\tilde{\sigma}_{G4}$	c4	93.97
5	$3 \cdot 10^3$	μ_L	94.50	−88.50	75	$5.30 \cdot 10^7$	$\tilde{\sigma}_{G4}$	c5	51.17
6	300	μ_A	72.57	−66.57	10	$9.42 \cdot 10^4$	-	c6	48.08
7	80	μ_C	49.62	−37.27	4.2	$4.43 \cdot 10^3$	$\tilde{\sigma}_{G5}$	c7	14.38
8	310	μ_E	31.23	25.23	11	$1.17 \cdot 10^5$	$\tilde{\sigma}_{G5}$	c8	8.92
9	40	μ_C	11.65	−5.65	4.2	$2.21 \cdot 10^3$	$\tilde{\sigma}_{G5}$	c9	5.44
10	50	μ_L	7.17	−1.18	12	$2.26 \cdot 10^4$	$\tilde{\sigma}_{G5}$	c10	50.52
11	$3 \cdot 10^3$	μ_L	5.40	0.60	150	$2.12 \cdot 10^8$	$\tilde{\sigma}_{G5}$	c11	47.51
12	260	μ_A	72.77	−66.77	10	$8.16 \cdot 10^4$	-	c12	12.94
13	100	μ_C	49.02	−35.35	4.2	$5.54 \cdot 10^3$	$\tilde{\sigma}_{G5}$	c13	9.88
14	265	μ_E	30.22	−24.22	11	$1.00 \cdot 10^5$	$\tilde{\sigma}_{G5}$	c14	9.12
15	210	μ_E	11.41	−5.41	9	$5.34 \cdot 10^4$	$\tilde{\sigma}_{G5}$	c15	7.78
16	60	μ_C	9.50	−3.50	4.2	$3.32 \cdot 10^3$	$\tilde{\sigma}_{G5}$	c16	5.37
17	210	μ_A	8.45	−2.45	9	$5.34 \cdot 10^4$	$\tilde{\sigma}_{G5}$	c17	4.41
18	30	μ_A	6.58	−0.58	12	$1.35 \cdot 10^4$	$\tilde{\sigma}_{G5}$	c18	4
19	$2 \cdot 10^3$	μ_L	4.89	1.11	190	$2.26 \cdot 10^8$	$\tilde{\sigma}_{G5}$	c19	12.36
20	$7 \cdot 10^3$	μ_L	4.20	1.79	425	$3.97 \cdot 10^9$	$\tilde{\sigma}_{G5}$	c20	11.73
21	-	-	12.36	−6.36	80	$2.14 \cdot 10^6$	$\tilde{\sigma}_{G2}$	c21	11.30
22	$14 \cdot 10^3$	μ_N	12.04	−6.04	15	$9.89 \cdot 10^6$	$\tilde{\sigma}_{G3}$	c22	10.93
23	$2 \cdot 10^3$	μ_N	11.51	−5.51	8.5	$4.53 \cdot 10^5$	$\tilde{\sigma}_{G3}$	c23	10.79
24	$2 \cdot 10^3$	μ_N	11.12	5.11	8.5	$4.53 \cdot 10^5$	$\tilde{\sigma}_{G3}$	c24	13.66
25	$3 \cdot 10^3$	μ_N	10.86	−4.86	12	$1.35 \cdot 10^6$	$\tilde{\sigma}_{G3}$	c25	12.90
26	$5 \cdot 10^3$	μ_N	10.73	−4.73	13.5	$2.86 \cdot 10^6$	$\tilde{\sigma}_{G3}$	c26	11.76
27	-	-	13.66	−7.66	100	$4.18 \cdot 10^6$	$\tilde{\sigma}_{G2}$	c27	10.84
28	$14 \cdot 10^3$	μ_N	13.28	−7.28	55	$9.89 \cdot 10^6$	$\tilde{\sigma}_{G3}$	c28	10.79
29	$5 \cdot 10^3$	μ_N	12.33	−6.33	8.5	$1.13 \cdot 10^6$	$\tilde{\sigma}_{G3}$	c29	10.66
30	$5 \cdot 10^3$	μ_N	11.30	−5.30	8.5	$1.13 \cdot 10^6$	$\tilde{\sigma}_{G3}$	c30	6.64
31	$1 \cdot 10^3$	μ_N	10.82	−4.82	12	$4.52 \cdot 10^5$	$\tilde{\sigma}_{G3}$	c31	2.00
32	$5 \cdot 10^3$	μ_N	10.73	−4.73	13.5	$2.86 \cdot 10^6$	$\tilde{\sigma}_{G3}$	c32	2
33	$1.5 \cdot 10^3$	μ_N	8.65	−2.65	16	$1.20 \cdot 10^6$	$\tilde{\sigma}_{G3}$		
34	$4.5 \cdot 10^3$	μ_N	4.32	1.68	16	$3.61 \cdot 10^6$	$\tilde{\sigma}_{G3}$		
35	$2.5 \cdot 10^3$	μ_N	2.00	4.00	2.3	$4.15 \cdot 10^{10}$	$\tilde{\sigma}_{G1}$		

Table 2. Parameter and reference values for the model compartments (indexed by i) and nodes (indexed by ci). Values for viscosity and flexibility are given in Table 3.

viscosity values (min·mmHg)	flexibility values (mmHg^{-1})
$\mu_L = 6.4 \cdot 10^{-7}$	$\tilde{\sigma}_{G1} = 0.002$
$\mu_A = \ 2 \cdot 10^{-6}$	$\tilde{\sigma}_{G2} = 0.005$
$\mu_E = 2.5 \cdot 10^{-6}$	$\tilde{\sigma}_{G3} = 0.045$
$\mu_C = 4.9 \cdot 10^{-6}$	$\tilde{\sigma}_{G4} = 0.004$
$\mu_N = 5.4 \cdot 10^{-8}$	$\tilde{\sigma}_{G5} = 0.065$

Table 3. Viscosity and flexibility values.

with either direct experimental measurements [Nyengaard 1993; Nordsletten et al. 2006; Jensen and Steven 1977; Heilmann et al. 2012; Cortes et al. 1996] or previous modeling studies [Moss and Layton 2014; Moss and Thomas 2014; Edwards and Layton 2011; Sgouralis and Layton 2012; 2013; 2016; Oien and Aukland 1991; Sgouralis et al. 2015; Chen et al. 2011].

The pressure-volume relationships used in the model, (10) and (20), require values for the parameters s_i. We assume that

(i) s_i scale proportionally to the reference volumes

$$s_i = \sigma_i V_i^{\mathrm{ref}}, \tag{21}$$

and

(ii) the coefficients σ_i depend only on the histology of the associated compartment.

That is, we group the compartments as follows:

*Group G*1: renal capsule (s_0) and papillary collecting duct (s_{35}),

*Group G*2: glomeruli (s_{21} and s_{27}),

*Group G*3: renal tubules (s_{22}–s_{26}) and proximal collecting ducts (s_{28}–s_{34}),

*Group G*4: preafferent arteriole blood vessels (s_3–s_5),

*Group G*5: postafferent arteriole blood vessels (s_7–s_{11} and s_{13}–s_{20}).

Then we assign the same flexibility value σ_i to all members of each group (Table 2). With this formulation, the model compartments in each histological group experience the same fractional change in volume whenever they are challenged by the same pressure gradient $P_i^{\mathrm{int}} - P_i^{\mathrm{ext}}$.

The available experimental data do not permit an accurate estimate of the values of the flexibility parameters. For this reason, we treat the flexibilities of the five groups σ_g as *independent random variables*. To facilitate the comparison among the different groups, we set

$$\sigma_g = \tilde{\sigma}_g \Lambda_g, \tag{22}$$

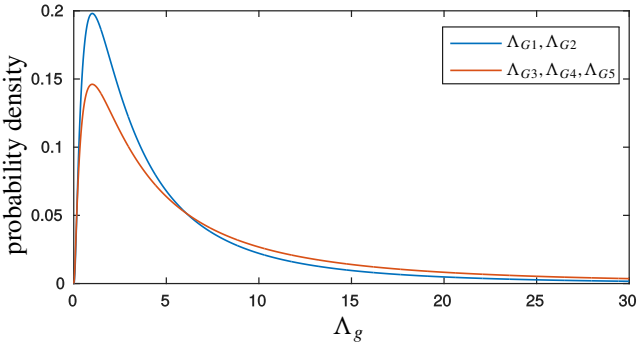


Figure 3. Probability densities of the flexibility parameters Λ_g of the histological groups G1–G5 used in this study.

where $\tilde{\sigma}_g$ are constants, and Λ_g are random variables configured to have mode 1. We estimate the values of $\tilde{\sigma}_g$ empirically based on ex vivo measurements reported in [Hebert et al. 1975; Zhu et al. 1992; Cortes et al. 1996; Cortell et al. 1973; Yamamoto et al. 1983] (Table 2).

For each simulation, Λ_g are drawn from the log-normal distribution (Figure 3), which is chosen such that

(i) s_g attain nonnegative values,

(ii) arbitrarily large values of s_g are allowed, and

(iii) low s_g values are more frequent than large ones.

We choose the latter condition assuming that the experimental procedures (anesthesia, renal decapsulation, tissue isolation, etc.) utilized in [Hebert et al. 1975; Cortes et al. 1996; Cortell et al. 1973; Yamamoto et al. 1983] likely increase rather than decrease tissue flexibility, thus our computed $\tilde{\sigma}_g$ likely overestimate rather than underestimate σ_g.

Finally, we configure the log-normal distributions such that Λ_{G1} and Λ_{G2} have a log-standard deviation of 1.1, and Λ_{G3}, Λ_{G4}, and Λ_{G5} have a log-standard deviation of 1.25 (Figure 3). According to our experience, such configuration reflects the degree of the uncertainty in our estimated values of $\tilde{\sigma}_g$, for which we consider $\tilde{\sigma}_{G3}$, $\tilde{\sigma}_{G4}$, and $\tilde{\sigma}_{G5}$ less accurately estimated than $\tilde{\sigma}_{G1}$ and $\tilde{\sigma}_{G2}$.

2.3. *Sensitivity analysis.*

2.3.1. *Formulation.* For the sensitivity analysis of the model described in the previous sections, we adopt a *variance-based method* which is best suited for nonlinear models [Saltelli et al. 2000; Sobol' 2001]. Let

$$y = f(x_1, x_2, \ldots, x_k) \tag{23}$$

denote a generic model, where y is an output value and $x_1, x_2, \ldots, x_k$ are some random inputs (in our case those represent the uncertain parameters). For a factor x_g, the first- and total-order sensitivity indices are given by

$$S_g = \frac{\mathbb{V}(\mathbb{E}(y \mid x_g))}{\mathbb{V}(y)}, \tag{24}$$

$$T_g = 1 - \frac{\mathbb{V}(\mathbb{E}(y \mid x_{-g}))}{\mathbb{V}(y)}, \tag{25}$$

respectively [Saltelli et al. 2000; Saltelli 2002; Sobol' 2001]. In the equations above, $\mathbb{E}$ and $\mathbb{V}$ denote mean value and variance, respectively. In (24), first the mean of y is computed by fixing the factor x_g to some value $\tilde{x}_g$, and then the variance of the mean values is computed over all possible $\tilde{x}_g$. In (25), first the mean value is computed by fixing all factors except x_g (which is denoted by x_{-g}), and then the variance of the mean values is computed over all possible x_{-g}.

According to the above definitions, the first-order index S_g indicates the fraction by which the variance of y will be reduced if only the value of the factor x_g is certainly specified [Saltelli et al. 2000]. Similarly, the total-order index T_g indicates the fraction of the variance of y that will be left if all factors besides x_g are certainly specified [Saltelli et al. 2000]. We compute both indices, because generally for a nonlinear model the factors are expected to interact in a nonadditive way, and therefore T_g is expected to be larger than S_g. The difference $T_g - S_g$ characterizes the extent of the interactions with the other factors that x_g is involved with.

2.3.2. *Evaluation of sensitivity indices.* To better characterize the contribution of the individual factors Λ_g of (22), in the variance of P_1 and P_2, we calculate their first- and total-order sensitivity indices given in (24) and (25). We compute the indices according to the method proposed by Saltelli [2002], which is computationally less demanding than a straightforward application of the formulas (24) and (25).

Briefly, according to the Saltelli method we form two input matrices:

$$M_A = \begin{bmatrix} \Lambda_{G1}^{1,A} & \Lambda_{G2}^{1,A} & \Lambda_{G3}^{1,A} & \Lambda_{G4}^{1,A} & \Lambda_{G5}^{1,A} & \Lambda_{G6}^{1,A} \\ \Lambda_{G1}^{2,A} & \Lambda_{G2}^{2,A} & \Lambda_{G3}^{2,A} & \Lambda_{G4}^{2,A} & \Lambda_{G5}^{2,A} & \Lambda_{G6}^{2,A} \\ \vdots & \vdots & \vdots & \vdots & \vdots & \vdots \\ \Lambda_{G1}^{N,A} & \Lambda_{G2}^{N,A} & \Lambda_{G3}^{N,A} & \Lambda_{G4}^{N,A} & \Lambda_{G5}^{N,A} & \Lambda_{G6}^{N,A} \end{bmatrix}, \tag{26}$$

$$M_B = \begin{bmatrix} \Lambda_{G1}^{1,B} & \Lambda_{G2}^{1,B} & \Lambda_{G3}^{1,B} & \Lambda_{G4}^{1,B} & \Lambda_{G5}^{1,B} & \Lambda_{G6}^{1,B} \\ \Lambda_{G1}^{2,B} & \Lambda_{G2}^{2,B} & \Lambda_{G3}^{2,B} & \Lambda_{G4}^{2,B} & \Lambda_{G5}^{2,B} & \Lambda_{G6}^{2,B} \\ \vdots & \vdots & \vdots & \vdots & \vdots & \vdots \\ \Lambda_{G1}^{N,B} & \Lambda_{G2}^{N,B} & \Lambda_{G3}^{N,B} & \Lambda_{G4}^{N,B} & \Lambda_{G5}^{N,B} & \Lambda_{G6}^{N,B} \end{bmatrix} \tag{27}$$

by generating Monte Carlo samples $\Lambda_g^{j,A}$ and $\Lambda_g^{j,B}$ for the factors Λ_g. Subsequently, for each factor, we form a matrix M_g. Each M_g is formed by the columns of M_A, except the column that corresponds to the factor Λ_g, which is taken from M_B. For instance, M_{G2} is given by

$$M_{G2} = \begin{bmatrix} \Lambda_{G1}^{1,A} & \boldsymbol{\Lambda_{G2}^{1,B}} & \Lambda_{G3}^{1,A} & \Lambda_{G4}^{1,A} & \Lambda_{G5}^{1,A} & \Lambda_{G6}^{1,A} \\ \Lambda_{G1}^{2,A} & \boldsymbol{\Lambda_{G2}^{2,B}} & \Lambda_{G3}^{2,A} & \Lambda_{G4}^{2,A} & \Lambda_{G5}^{2,A} & \Lambda_{G6}^{2,A} \\ \vdots & \vdots & \vdots & \vdots & \vdots & \vdots \\ \Lambda_{G1}^{N,A} & \boldsymbol{\Lambda_{G2}^{N,B}} & \Lambda_{G3}^{N,A} & \Lambda_{G4}^{N,A} & \Lambda_{G5}^{N,A} & \Lambda_{G6}^{N,A} \end{bmatrix}. \tag{28}$$

We use each row of the matrices M_A, M_B, and M_g to solve the model equations at $P_a = 180\,\text{mmHg}$ and combine the solutions in the vectors

$$m_A^k = \begin{bmatrix} P_k^{1,A} \\ P_k^{2,A} \\ \vdots \\ P_k^{N,A} \end{bmatrix}, \qquad m_B^k = \begin{bmatrix} P_k^{1,B} \\ P_k^{2,B} \\ \vdots \\ P_k^{N,B} \end{bmatrix}, \qquad m_g^k = \begin{bmatrix} P_k^{1,g} \\ P_k^{2,g} \\ \vdots \\ P_k^{N,g} \end{bmatrix}, \tag{29}$$

where $k = 1$ corresponds to the pressure in the cortical region P_1, and $k = 2$ to the pressure in the medullary region P_2. The first- and total-order sensitivity indices are then computed by

$$S_g^k = \frac{1/(N-1)\sum_{j=1}^N (P_k^{j,A} P_k^{j,g}) - 1/N \sum_{j=1}^N (P_k^{j,A} P_k^{j,B})}{\mathbb{V}(m_A^k)}, \tag{30}$$

$$T_g^k = 1 - \frac{1/(N-1)\sum_{j=1}^N (P_k^{j,B} P_k^{j,g}) - \left(1/N \sum_{j=1}^N P_k^{j,B}\right)^2}{\mathbb{V}(m_B^k)}, \tag{31}$$

respectively. In (30) and (31), $\mathbb{V}$ denotes the sample variance. For further details on the method, see [Saltelli 2002].

2.4. ***Numerical methods.*** For the numerical solution, we combine the model equations (1)–(20) into a system of 69 coupled nonlinear equations. Given a value for the arterial blood pressure P_a and a choice for the flexibility parameters Λ_g, the resulting system is solved to yield the values for the pressures at the interstitial regions P_1 and P_2, the pressures at the model nodes P_{c1}–P_{c32}, and the volumes of the compartments V_1–V_{35}.

To obtain solutions, we implement the system in MATLAB and use the standard root-finding function (fsolve). This function computes solutions to the model equations iteratively by starting from a given initial approximation. For the initial approximation we use the reference values from literature (Table 2). Note that by

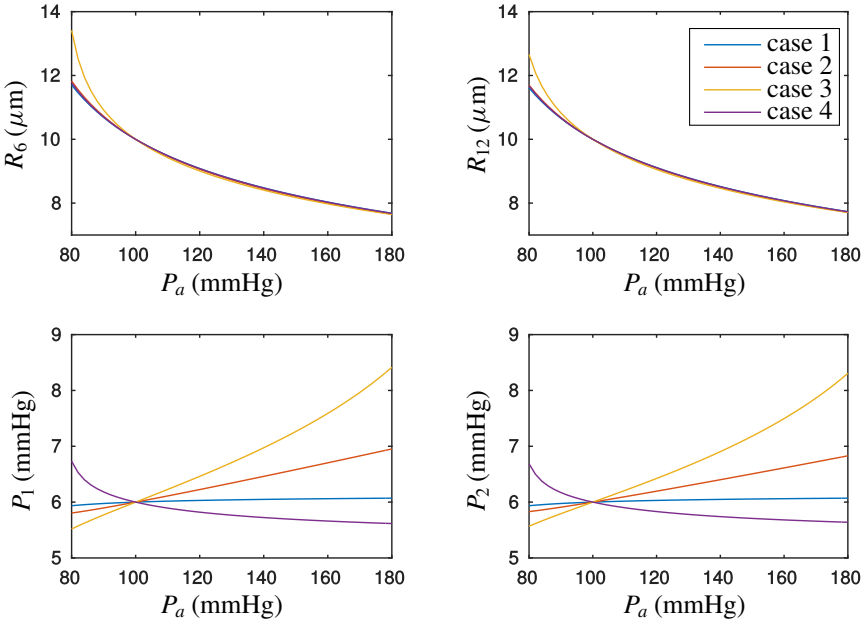


Figure 4. Model predictions for selected parameter choices. Upper panels: radii of the afferent arterioles. Lower panels: pressures in the interstitial regions.

the construction of the model, the solution at reference can be obtained trivially, and thus no root-finding is necessary for this step.

3. Results

3.1. ***Selected case studies.*** In the first set of simulations, we investigate how the pressures in the interstitial regions P_1 and P_2 are affected by the arterial blood pressure P_a for selected choices of the flexibility parameters when P_a varies in the range 80–180 mmHg. In particular, we make the following choices for the flexibility parameters:

Case 1: $\Lambda_{G1} = \Lambda_{G2} = \Lambda_{G3} = \Lambda_{G4} = \Lambda_{G5} = 0$,

Case 2: $\Lambda_{G1} = \Lambda_{G2} = \Lambda_{G3} = \Lambda_{G4} = \Lambda_{G5} = 1$,

Case 3: $\Lambda_{G1} = \Lambda_{G2} = \Lambda_{G3} = \Lambda_{G4} = \Lambda_{G5} = 4$,

Case 4: $\Lambda_{G3} = 0$ and $\Lambda_{G4} = 0.27$ and $\Lambda_{G5} = 0.2$.

Figure 4 shows key solution values.

Case 1 corresponds to a kidney with rigid compartments. In this case, pressure does not affect the volume of the compartments except for the two afferent arterioles V_6 and V_{12}. For example, at elevated P_a, the pressure differences along the afferent arterioles $P_{c4} - P_{c5}$ and $P_{c3} - P_{c10}$ increase. As a result, the arterioles constrict in order to maintain constant blood flow; see (12) and (13). Given that total kidney volume V_0, given by (20), does not change, the reduction in afferent arteriole volume increases the volume of the interstitial regions V_1 and V_2 given by (18). In turn, increases in interstitial volumes reduce the protein concentrations C_1 and C_2 by (16) and (17) and the oncotic pressures π_1 and π_2 that promote uptake J_9 and J_{16} of interstitial fluid by (4) and (5). However, due to tubular reabsorption J_{22}–J_{34}, the flow of fluid into the interstitial spaces is kept constant; see (14) and (15). Thus, in order to maintain a constant uptake and avoid accumulation of interstitial fluid, P_1 and P_2 increase. Vice versa, a decrease in P_a has the opposite effect and results in a decrease of P_1 and P_2. Because the total volume of the afferent arterioles is only a minor fraction of the volume of the interstitial regions ($\sim 2\%$, see Table 2), even large changes in R_6 and R_{12} induce small changes in π_1 and π_2. Therefore, the total change in P_1 and P_2, across the full range of P_a variation, is in the order of 0.1 mmHg (see blue curves in Figure 4).

Case 2 corresponds to a kidney with distensible compartments. This case is similar to Case 3; however, the changes in P_1 induced by the constriction of the afferent arterioles is followed by an expansion of the renal capsule (20), which increases whole kidney volume V_0. In this case, the cortical and medullary interstitial volumes V_1 and V_2 increase to a larger extent compared with Case 1 in order to accommodate the expansion of V_0. As a result, interstitial protein concentrations C_1 and C_2, and oncotic pressures π_1 and π_2 drop by larger amounts than in Case 1. Consequently, significant drops in P_1 and P_2 follow (see orange curves in Figure 4).

Case 3 corresponds to a kidney with very flexible compartments and renal capsule. Through the same effects as in Cases 1 and 2, changes in arterial pressure P_a lead to similar changes in P_1 and P_2. Because in this case the expansion of whole kidney volume V_0 is greater than in Case 2, due to the increased flexibility of the renal capsule s_0, the interstitial pressures are affected to a greater extent (see yellow curves in Figure 4).

Case 4 shows a different behavior that corresponds to a kidney with a flexible capsule but relatively rigid compartments. As in all cases, P_a affects severely the pressures in the preafferent arteriole vascular compartments P_3, P_4, and P_5 — see (11) — which are not regulated by the active constriction/dilation of the afferent arterioles. As a result, whenever P_a increases, P_3, P_4, and P_5 also increase, leading to an increase of the associated preafferent arteriole vascular volumes V_3, V_4, and V_5. Note that the increase of V_3, V_4, and V_5 opposes the reduction of V_6 and V_{12} caused by constriction of the afferent arterioles. In this particular case, opposite to

what happens in Cases 1–3, the increase of the total volume of the preafferent arteriole compartments V_3, V_4, and V_5 exceeds the reduction of the total volume of the afferent arterioles V_6 and V_{12}. As a result, the interstitial regions are compressed, which in turn leads to increases of the protein concentrations C_1 and C_2 and oncotic pressures π_1 and π_2. Because the uptake of interstitial fluid is maintained constant, this leads to reductions of P_1 and P_2. Finally, the reductions of P_1 and P_2 are further amplified by constriction of the renal capsule that follows the reduction of P_1.

3.2. ***Sensitivity analysis.*** From the previous section, it is apparent that the predictions of the model depend on the choice of the flexibility parameters Λ_g, which are not well-characterized (Section 2.2). To assess the degree to which different choices affect the pressures in the interstitial regions P_1 and P_2, we sample the parameter space. For each sample point, we evaluate the model solution at an elevated arterial blood pressure P_a. For all simulations, we keep P_a constant at 180 mmHg.

3.2.1. *Summary statistics.* The model utilizes five factors that correspond to the flexibility parameters associated with the histological groups of Section 2.2. We use a sample size of $N = 41 \cdot 10^3$ and perform sampling with the Monte Carlo method. The resulting probability densities and cumulative distributions of P_1 and P_2 are shown in Figure 5.

As can be seen in Figure 5, the model predicts mostly increased P_1 and P_2 at elevated P_a. However, the uncertainty in the flexibility parameters Λ_g induces a significant degree of variability for both pressures. The mean values of P_1 and P_2 are 9.1 and 8.6 mmHg, and the standard deviations are 4.1 and 3.7 mmHg, respectively. Both pressure distributions are heavily skewed towards large values.

Interestingly, the model also predicts low or even negative pressures. Negative pressure values indicate that the pressures in the interstitial regions fall below the pressure in the space surrounding the kidney P_0^{ext}, which in this study is set to 0 mmHg. In summary, 84% of P_1 and 77% of P_2 values at $P_a = 180$ mmHg are above the corresponding values at $P_a = 100$ mmHg, and 16% of P_1 and 11% of P_2 values lie below 0 mmHg or above 15 mmHg.

Scatter plots between the input factors Λ_g and the computed pressures P_1 and P_2 are shown in Figure 6. Only Λ_{G4} shows a clear influence on P_1 and P_2, with high values of Λ_{G4} being associated generally with higher interstitial pressures. No apparent trend can be identified for the rest of the factors. Linear regressions between the computed pressures and the input factors (shown by the dashed lines in Figure 6) yield low R^2. Precisely, values of R^2 for Λ_{G4} equal 0.25 for P_1 and 0.16 for P_2. The rest of the factors yield R^2 for 0.02 or less. Such low R^2 indicate strong nonlinear dependencies of the interstitial pressures on the input factors, a behavior that most likely stems from the inverse-forth-power in the Poiseuille law given by (11).

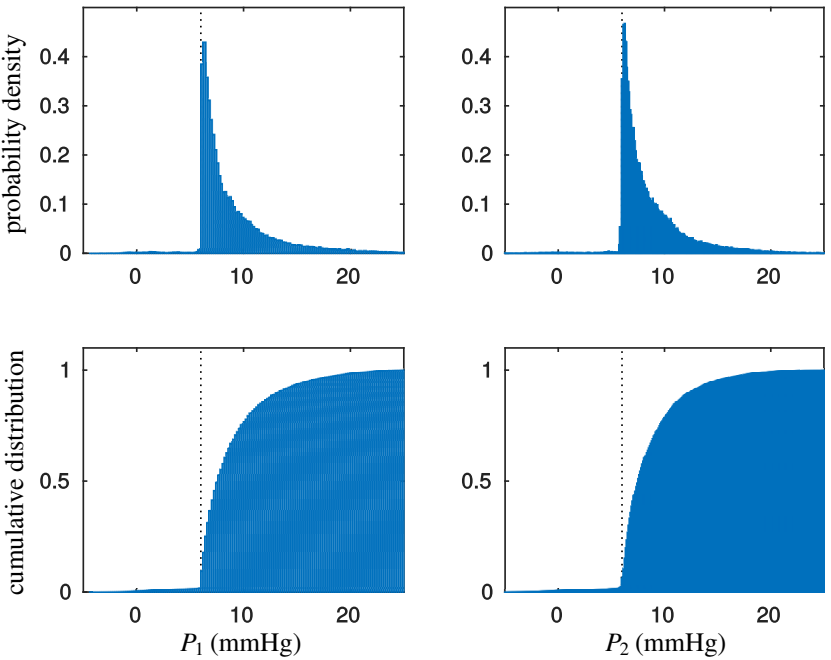


Figure 5. Probability densities of P_1, left panels, and P_2, right panels, at elevated arterial blood pressure ($P_a = 180$ mmHg) as estimated by model simulations. Vertical lines indicate the values at the reference arterial blood pressure ($P_a = 100$ mmHg).

Correlation coefficients computed between the input factors Λ_g and the computed pressures P_1 and P_2 are shown in Figure 7, left panels. As is suggested by Figure 6, Λ_{G4} is positively correlated (weakly) with P_1 and P_2. From the rest of the factors, Λ_{G1}, Λ_{G3}, and Λ_{G5} are negatively correlated with P_1 and P_2 to an even weaker extent than for Λ_{G4}, and Λ_{G2} shows no correlation with either P_1 or P_2.

In contrast to the apparent lack of any trend between the computed pressures P_1 and P_2 and the input factors Λ_{G4}, the model predicts a high degree of correlation between P_1 and P_2. The associated correlation coefficient reaches as high as 0.95 (Figure 7 right panels), which indicates that P_1 and P_2 are predicted to change *in tandem* in a seemingly linear way.

3.2.2. *Sensitivity indices.* To better characterize the contribution of the individual factors Λ_g in the variance of P_1 and P_2, we calculate their first- and total-order sensitivity indices shown in (24) and (25). Details on the adopted computational methods can be found in Section 2.3.

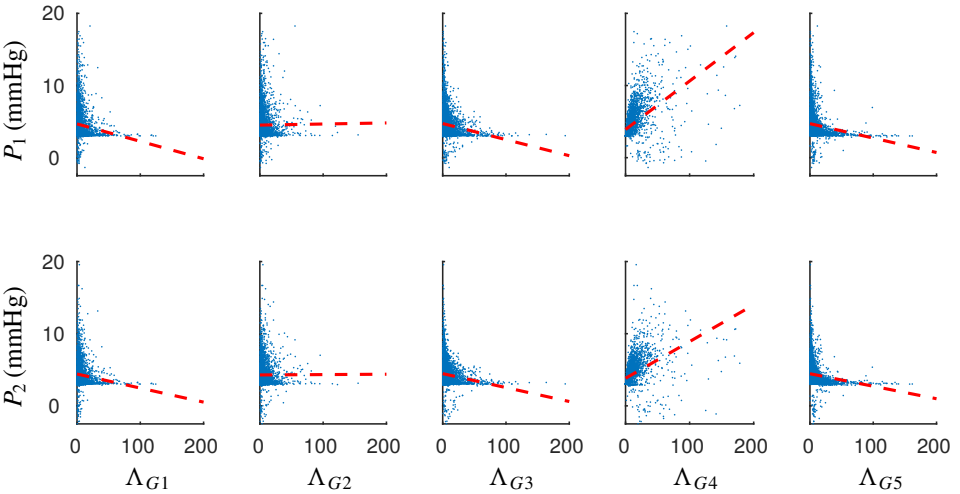


Figure 6. Interstitial pressures P_1, upper panels, and P_2, lower panels, with respect to the sampled input factors Λ_g. Dashed lines indicate the linear regression estimates. For clarity, only $\frac{1}{5}$ of the computed points are shown.

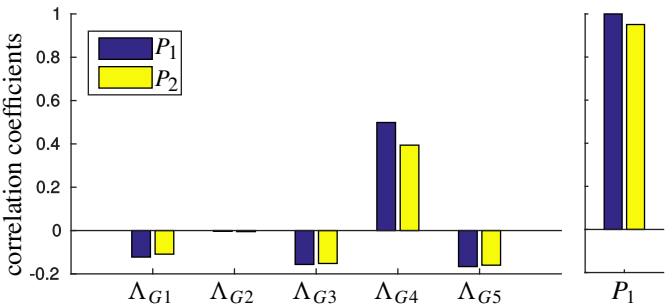


Figure 7. Correlation coefficients between the input factors Λ_g and the computed pressures in the cortical and medullary interstitial spaces P_1 and P_2, respectively.

Figure 8 shows the computed indices. Evidently, the flexibility of the preafferent arteriole vascular segments (group G4) accounts for most of the variation in P_1 or P_2 with respect to either the first- or total-order indices. The postafferent arteriole vasculature (group G5) has the second-most significant contribution. Groups G1–G3 have only minor contributions according to the first-order sensitivity indices. However, this is not the case with the total-order indices, which indicate that G1 and G3 are involved to a significant degree in interactions. On the contrary, the glomeruli (group G2) have only a minor involvement in interactions.

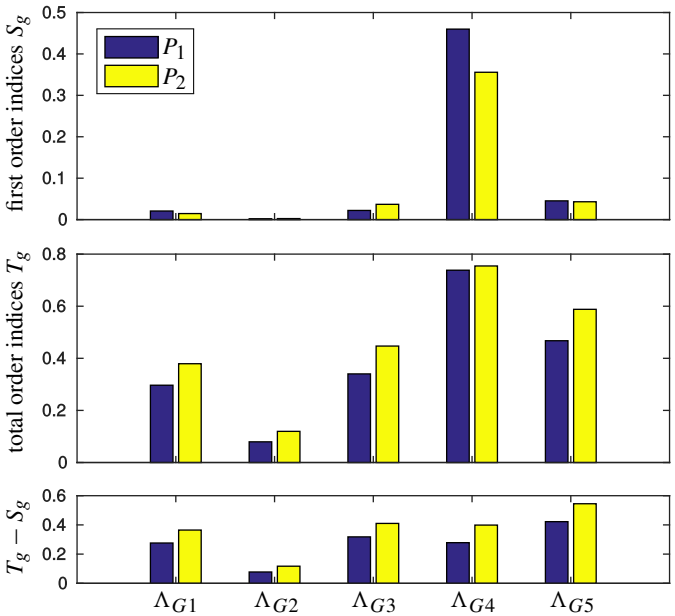


Figure 8. First-order, upper panel, and total-order, middle panel, sensitivity indices of P_1 and P_2 at elevated arterial blood pressure ($P_a = 180$ mmHg). Lower panel shows the difference between the first- and total-order sensitivity indices.

For all groups, it is observed that $T_g^1 < T_g^2$ and $T_g^1 - S_g^1 < T_g^2 - S_g^2$, which indicate that the medullary pressure P_2 is more susceptible to interactions than cortical pressure P_1. This behavior is expected, given that the afferent arterioles (compartments 6 and 12), which initiate the changes in P_1 and P_2, are located exclusively in the cortex, while the medulla is susceptible mostly to secondary interactions initiated by the expansion/constriction of the renal capsule.

4. Conclusions

We developed a multicompartmental computational model of the rat kidney. The model is constructed using conservation laws (2) and (7), fluid dynamics (11), simplified pressure-volume relationships (10) and (20), and constitutive equations specific to the physiology of the kidney (3) and (14) and (15).

We assigned values to the model parameters (Tables 1 and 2) using experimental measurements when such measurements were available and previous modeling studies when direct measurements were not available. However, the data required

for the flexibility parameters σ_i are sparse and do not suffice for an accurate estimation of their values. To that end, we chose to model these parameters as random variables with probability distributions that permit values spanning multiple orders of magnitude (Section 2.2 and Figure 3).

To determine the probability distributions of the random variables, we defined five histological groups within the model kidney. Group $G1$ models thick and relatively inflexible structures, for which we used pressure-mass data obtained from whole kidneys in dogs [Hebert et al. 1975; Zhu et al. 1992]. Group $G2$ models the glomeruli, for which we used pressure-volume data measured in rats [Cortes et al. 1996]. Group $G3$ models the various segments of the nephrons and the proximal parts of the collecting duct, for which we used pressure-radius measurements of the rat proximal tubule [Cortell et al. 1973]. Groups $G4$ and $G5$ model the blood vessels, for which we used pressure-volume measurements of the systemic circulation measured in rats [Yamamoto et al. 1983]. We combined the postafferent arteriole vasculature in one group (group $G5$), despite that it consists of segments of the arterial and venous vascular trees [Kriz and Bankir 1988]. We were motivated to do so by the fact that these vascular segments have considerably thinner walls and therefore should be considerably more flexible than the preafferent arteriole segments [Rhodin 1980].

Output from the model leads to a range of predictions depending on the choices of the flexibility values. Generally, increased arterial blood pressure is predicted to increase the pressure in both interstitial spaces (Figure 5). As arterial blood pressure increases from 100 mmHg to 180 mmHg, interstitial pressures are predicted to increase on average by ~ 3 mmHg. Changes of similar magnitude have been observed in the kidneys of rats [Garcia-Estan and Roman 1989; Khraibi et al. 2001; Skarlatos et al. 1994; Khraibi 2000] and dogs [Majid et al. 2001; Granger and Scott 1988]. Upon a limited number of flexibility choices, however, the model predicts decreased interstitial pressures as a result. Furthermore, the model predicts a tight correlation between the cortical and the medullary pressures (Figure 7, right panels) which is also in agreement with the experimental observations reported in [Garcia-Estan and Roman 1989]. Concerning the four case studies of Section 3.1, Cases 2 and 3 are in best agreement with the experimental observations in [Garcia-Estan and Roman 1989; Khraibi et al. 2001; Skarlatos et al. 1994; Khraibi 2000; Majid et al. 2001; Granger and Scott 1988]. In contrast, Case 4 deviates from the experimental observations.

As arterial blood pressure P_a increases, mainly two distinct pathways that lead to interstitial pressure P_1 and P_2 changes can be identified (Figure 9). The first pathway (denoted with red) leads to an *increase* of interstitial pressure upon constriction of the afferent arterioles. The second pathway (denoted with blue) leads to a *decrease* of interstitial pressure upon dilation of the preafferent arteriole blood

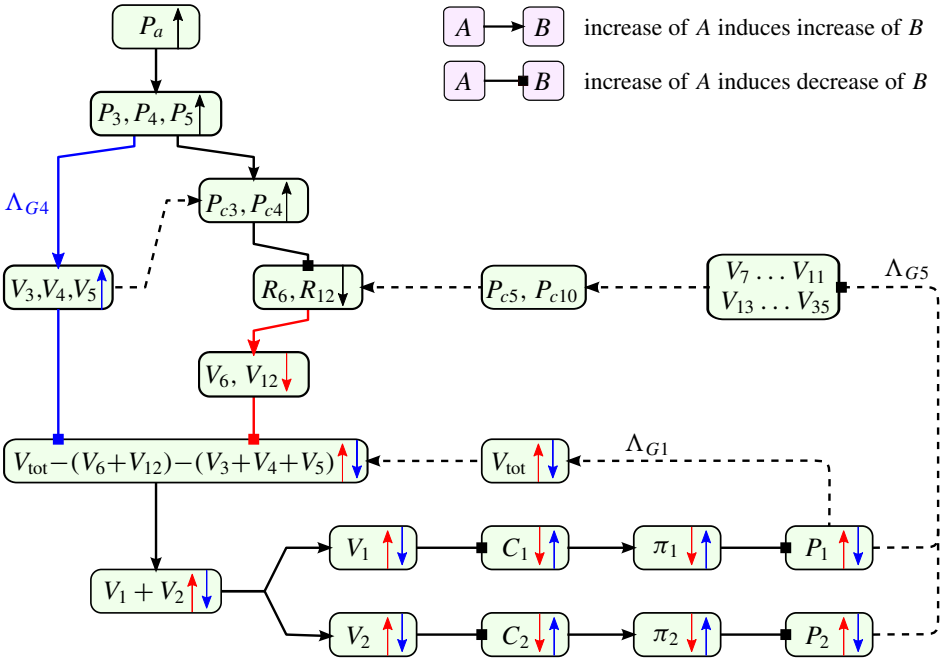


Figure 9. A summary of the mechanism relating arterial blood pressure P_a and interstitial pressures P_1 and P_2. Changes in P_a are transmitted to P_1 and P_2 primarily by two pathways: one is mediated by afferent arteriole volumes (V_6, V_{12}) which is marked with red arrows, the other is mediated by preafferent arteriole volumes (V_3, V_4, V_5) and is marked with blue arrows. The two pathways have competing effects. Secondary interactions are denoted with dashed lines. For simplicity, some of the secondary interactions are omitted.

vessels. Primarily, both pathways lead to changes in interstitial volumes V_1 and V_2, which are subsequently transmitted to protein concentrations C_1 and C_2, oncotic pressures π_1 and π_2, and finally to P_1 and P_2. The two pathways have competing effects; the first leads to changes of P_1 and P_2 towards the same direction as P_a, while the second leads to changes of P_1 and P_2 towards the opposite direction of P_a. It is important to note that, in general, both pathways are active. However, the model results (Figure 5) indicate that under most circumstances the first pathway dominates over the second.

The model predictions appear particularly sensitive to the flexibility of the preafferent arteriole blood vessels (histological group G4) (Figure 8). Such behavior is attributed mostly to the fact that blood pressure is only regulated by the afferent arterioles, which are located after these vessels [Sgouralis and Layton 2015].

The lack of pressure regulation, in the preafferent arteriole compartments, leads to larger internal pressure P_i^{int} changes upon increases in arterial pressure P_a than in the rest of the compartments. For example, as P_a increases from 100 mmHg to 180 mmHg, assuming an increase in the interstitial pressures of ~ 5 mmHg, we see that the compartments of group G4 are stretched by a pressure difference of ~ 70–75 mmHg, while the walls of the rest of the compartments are stretched by a pressure difference of ~ 5 mmHg. Thus, in view of the pressure-volume relations given by (10), the resulting change in total kidney volume V_0, which mediates the changes in interstitial pressures, is mostly affected by s_{G4} rather than s_{G1}, s_{G2}, s_{G3}, or s_{G5}.

The model developed in this study uses several simplifications. For example, the current model assumes perfect autoregulation of blood flow for equations (12) and (13), which limits its applicability to cases with arterial blood pressures between 80 mmHg and 180 mmHg [Sgouralis and Layton 2015]. The model does not account for the differences in tubular reabsorption, e.g., coefficients f_i in (3), occurring between diuretic and antidiuretic animals or for pressure-diuretic responses [Cowley 1997; Moss and Thomas 2014]. Furthermore, the model assumes linear pressure-volume relationships for (10) and (20). Lifting those limitations requires a more detailed model, the development of which will be the focus of future studies. Despite these limitations, the present model could be a useful component in comprehensive models of renal physiology.

Acknowledgments

The authors thank Dr. Vasileios Maroulas for assistance with the statistical analysis in this study and for other helpful discussions. This work is conducted as a part of the 2015 Summer Research Experience for Undergraduates and Teachers at the National Institute for Mathematical and Biological Synthesis (NIMBioS), sponsored by the National Science Foundation through NSF Award #DBI-1300426, with additional support from The University of Tennessee, Knoxville.

References

[Chen et al. 2011] J. Chen, I. Sgouralis, L. C. Moore, H. E. Layton, and A. T. Layton, "A mathematical model of the myogenic response to systolic pressure in the afferent arteriole", *Am. J. Physiol. Renal Physiol.* **300**:3 (2011), F669–F681.

[Cortell et al. 1973] S. Cortell, F. J. Gennari, M. Davidman, W. H. Bossert, and W. B. Schwartz, "A definition of proximal and distal tubular compliance: practical and theoretical implications", *J. Clin. Invest.* **52**:9 (1973), 2330–2339.

[Cortes et al. 1996] P. Cortes, X. Zhao, B. L. Riser, and R. G. Narins, "Regulation of glomerular volume in normal and partially nephrectomized rats", *Am. J. Physiol. Renal Physiol.* **270**:2 (1996), F356–F370.

[Cowley 1997] A. W. Cowley, "Role of the renal medulla in volume and arterial pressure regulation", *Am. J. Physiol. Regul. Integr. Comp. Physiol.* **273**:1 (1997), R1–R15.

[Deen et al. 1972] W. M. Deen, C. R. Robertson, and B. M. Brenner, "A model of glomerular ultrafiltration in the rat", *Am. J. Physiol. Legacy* **223**:5 (1972), 1178–1183.

[Eaton et al. 2009] D. C. Eaton, J. Pooler, and A. J. Vander, *Vander's renal physiology*, 7th ed., McGraw-Hill, New York, 2009.

[Edwards and Layton 2011] A. Edwards and A. T. Layton, "Modulation of outer medullary NaCl transport and oxygenation by nitric oxide and superoxide", *Am. J. Physiol. Renal Physiol.* **301**:5 (2011), F979–F996.

[Fry et al. 2014] B. C. Fry, A. Edwards, I. Sgouralis, and A. T. Layton, "Impact of renal medullary three-dimensional architecture on oxygen transport", *Am. J. Physiol. Renal Physiol.* **307**:3 (2014), F263–F272.

[Garcia-Estan and Roman 1989] J. Garcia-Estan and R. J. Roman, "Role of renal interstitial hydrostatic pressure in the pressure diuresis response", *Am. J. Physiol. Renal Physiol.* **256**:1 (1989), F63–F70.

[Granger and Scott 1988] J. P. Granger and J. W. Scott, "Effects of renal artery pressure on interstitial pressure and Na excretion during renal vasodilation", *Am. J. Physiol. Renal Physiol.* **255**:5 (1988), F828–F833.

[Hebert et al. 1975] L. A. Hebert, K. A. Stuart, and J. A. Stemper, "Whole kidney volume/pressure relationships", *Kidney Int.* **7**:1 (1975), 45–54.

[Heilmann et al. 2012] M. Heilmann, S. Neudecker, I. Wolf, L. Gubhaju, C. Sticht, D. Schock-Kusch, W. Kriz, J. F. Bertram, L. R. Schad, and N. Gretz, "Quantification of glomerular number and size distribution in normal rat kidneys using magnetic resonance imaging", *Nephrol. Dial. Transplant.* **27**:1 (2012), 100–107.

[Holstein-Rathlou and Marsh 1994] N. H. Holstein-Rathlou and D. J. Marsh, "Renal blood flow regulation and arterial pressure fluctuations: a case study in nonlinear dynamics", *Physiol. Reviews* **74**:3 (1994), 637–681.

[Jensen and Steven 1977] P. K. Jensen and K. Steven, "Angiotensin II induced reduction of peritubular capillary diameter in the rat kidney", *Pflügers Archiv* **371**:3 (1977), 245–250.

[Khraibi 2000] A. A. Khraibi, "Renal interstitial hydrostatic pressure and pressure natriuresis in pregnant rats", *Am. J. Physiol. Renal Physiol.* **279**:2 (2000), F353–F357.

[Khraibi et al. 2001] A. A. Khraibi, M. Liang, and T. J. Berndt, "Role of gender on renal interstitial hydrostatic pressure and sodium excretion in rats", *Am. J. Hypertens.* **14**:9 (2001), 893–896.

[Kriz and Bankir 1988] W. Kriz and L. Bankir, "A standard nomenclature for structures of the kidney", *Kidney Int.* **33**:1 (1988), 1–7.

[Layton et al. 2012] A. T. Layton, P. Pham, and H. Ryu, "Signal transduction in a compliant short loop of Henle", *Int. J. Numer. Methods Biomed. Eng.* **28**:3 (2012), 369–383. MR Zbl

[Majid et al. 2001] D. S. A. Majid, K. E. Said, S. A. Omoro, and L. G. Navar, "Nitric oxide dependency of arterial pressure-induced changes in renal interstitial hydrostatic pressure in dogs", *Circul. Res.* **88**:3 (2001), 347–351.

[Moffat and Fourman 1963] D. B. Moffat and J. Fourman, "A vascular pattern of the rat kidney", *J. Anat. Lond.* **97** (1963), 543–553.

[Moss and Layton 2014] R. Moss and A. T. Layton, "Dominant factors that govern pressure natriuresis in diuresis and antidiuresis: a mathematical model", *Am. J. Physiol. Renal Physiol.* **306**:9 (2014), F952–F969.

[Moss and Thomas 2014] R. Moss and S. R. Thomas, "Hormonal regulation of salt and water excretion: a mathematical model of whole kidney function and pressure natriuresis", *Am. J. Physiol. Renal Physiol.* **306**:2 (2014), F224–F248.

[Nordsletten et al. 2006] D. A. Nordsletten, S. Blackett, M. D. Bentley, E. L. Ritman, and N. P. Smith, "Structural morphology of renal vasculature", *Am. J. Physiol. Heart Circul. Physiol.* **291**:1 (2006), H296–H309.

[Nyengaard 1993] J. R. Nyengaard, "Number and dimensions of rat glomerular capillaries in normal development and after nephrectomy", *Kidney Internat.* **43**:5 (1993), 1049–1057.

[Oien and Aukland 1991] A. H. Oien and K. Aukland, "A multinephron model of renal blood flow autoregulation by tubuloglomerular feedback and myogenic response", *Acta Physiol. Scand.* **143**:1 (1991), 71–92.

[Rhodin 1980] J. A. G. Rhodin, "Architecture of the vessel wall", pp. 1–31 in *Handbook of physiology, supplement 7: The cardiovascular system, vascular smooth muscle*, American Physiological Society, Bethesda, MD, 1980.

[Saltelli 2002] A. Saltelli, "Making best use of model evaluations to compute sensitivity indices", *Comput. Phys. Commun.* **145**:2 (2002), 280–297. Zbl

[Saltelli et al. 2000] A. Saltelli, S. Tarantola, and F. Campolongo, "Sensitivity analysis as an ingredient of modeling", *Statist. Sci.* **15**:4 (2000), 377–395. MR

[Sgouralis and Layton 2012] I. Sgouralis and A. T. Layton, "Autoregulation and conduction of vasomotor responses in a mathematical model of the rat afferent arteriole", *Am. J. Physiol. Renal Physiol.* **303**:2 (2012), F229–F239.

[Sgouralis and Layton 2013] I. Sgouralis and A. T. Layton, "Control and modulation of fluid flow in the rat kidney", *Bull. Math. Biol.* **75**:12 (2013), 2551–2574. MR Zbl

[Sgouralis and Layton 2014] I. Sgouralis and A. T. Layton, "Theoretical assessment of renal autoregulatory mechanisms", *Am. J. Physiol. Renal Physiol.* **306**:11 (2014), F1357–F1371.

[Sgouralis and Layton 2015] I. Sgouralis and A. T. Layton, "Mathematical modeling of renal hemodynamics in physiology and pathophysiology", *Math. Biosci.* **264** (2015), 8–20. MR Zbl

[Sgouralis and Layton 2016] I. Sgouralis and A. T. Layton, "Conduction of feedback-mediated signal in a computational model of coupled nephrons", *Math. Med. Biol.* **33**:1 (2016), 87–106. MR Zbl

[Sgouralis et al. 2015] I. Sgouralis, R. G. Evans, B. S. Gardiner, J. A. Smith, B. C. Fry, and A. T. Layton, "Renal hemodynamics, function, and oxygenation during cardiac surgery performed on cardiopulmonary bypass: a modeling study", *Physiol. Rep.* **3**:1 (2015).

[Skarlatos et al. 1994] S. Skarlatos, P. H. Brand, P. J. Metting, and S. L. Britton, "Spontaneous changes in arterial blood pressure and renal interstitial hydrostatic pressure in conscious rats", *J. Physiol.* **481**:3 (1994), 743–752.

[Sobol' 2001] I. M. Sobol', "Global sensitivity indices for nonlinear mathematical models and their Monte Carlo estimates", *Math. Comput. Simulation* **55**:1-3 (2001), 271–280. MR Zbl

[Wolgast et al. 1981] M. Wolgast, M. Larson, and K. Nygren, "Functional characteristics of the renal interstitium", *Am. J. Physiol. Renal Physiol.* **241**:2 (1981), F105–F111.

[Yamamoto et al. 1983] J. Yamamoto, Y. Goto, M. Nakai, K. Ogino, and M. Ikeda, "Circulatory pressure-volume relationship and cardiac output in DOCA-salt rats", *Hypertension* **5**:4 (1983), 507–513.

[Zhu et al. 1992] M. Q. Zhu, W. Vaneerdeweg, N. Buyssens, and M. E. De Broe, "Quantitative relationships between body weight, kidney weight and nephron size in mongrel dogs", *Nephron* **62**:2 (1992), 187–191.

Received: 2015-09-29 Revised: 2016-04-26 Accepted: 2016-07-11

mbedell@andrew.cmu.edu *Carnegie Mellon University, 5000 Forbes Ave., Pittsburgh, PA 15213, United States*

claire.lin@emory.edu *Emory University, 201 Dowman Dr., Atlanta, GA 30322, United States*

roman.melendez2104@gmail.com *University of Puerto Rico Mayaguez, 259 Blvd. Alfonso Valdez Cabian, Mayagüez 00680, Puerto Rico*

sgouralis@nimbios.org *National Institute for Mathematical and Biological Synthesis (NIMBioS), University of Tennessee, 1122 Volunteer Blvd., Suite 106, Knoxville, TN 37996, United States*

involve

msp.org/involve

INVOLVE YOUR STUDENTS IN RESEARCH

Involve showcases and encourages high-quality mathematical research involving students from all academic levels. The editorial board consists of mathematical scientists committed to nurturing student participation in research. Bridging the gap between the extremes of purely undergraduate research journals and mainstream research journals, *Involve* provides a venue to mathematicians wishing to encourage the creative involvement of students.

MANAGING EDITOR

Kenneth S. Berenhaut Wake Forest University, USA

BOARD OF EDITORS

Colin Adams	Williams College, USA	Suzanne Lenhart	University of Tennessee, USA
John V. Baxley	Wake Forest University, NC, USA	Chi-Kwong Li	College of William and Mary, USA
Arthur T. Benjamin	Harvey Mudd College, USA	Robert B. Lund	Clemson University, USA
Martin Bohner	Missouri U of Science and Technology, USA	Gaven J. Martin	Massey University, New Zealand
Nigel Boston	University of Wisconsin, USA	Mary Meyer	Colorado State University, USA
Amarjit S. Budhiraja	U of North Carolina, Chapel Hill, USA	Emil Minchev	Ruse, Bulgaria
Pietro Cerone	La Trobe University, Australia	Frank Morgan	Williams College, USA
Scott Chapman	Sam Houston State University, USA	Mohammad Sal Moslehian	Ferdowsi University of Mashhad, Iran
Joshua N. Cooper	University of South Carolina, USA	Zuhair Nashed	University of Central Florida, USA
Jem N. Corcoran	University of Colorado, USA	Ken Ono	Emory University, USA
Toka Diagana	Howard University, USA	Timothy E. O'Brien	Loyola University Chicago, USA
Michael Dorff	Brigham Young University, USA	Joseph O'Rourke	Smith College, USA
Sever S. Dragomir	Victoria University, Australia	Yuval Peres	Microsoft Research, USA
Behrouz Emamizadeh	The Petroleum Institute, UAE	Y.-F. S. Pétermann	Université de Genève, Switzerland
Joel Foisy	SUNY Potsdam, USA	Robert J. Plemmons	Wake Forest University, USA
Errin W. Fulp	Wake Forest University, USA	Carl B. Pomerance	Dartmouth College, USA
Joseph Gallian	University of Minnesota Duluth, USA	Vadim Ponomarenko	San Diego State University, USA
Stephan R. Garcia	Pomona College, USA	Bjorn Poonen	UC Berkeley, USA
Anant Godbole	East Tennessee State University, USA	James Propp	U Mass Lowell, USA
Ron Gould	Emory University, USA	Józeph H. Przytycki	George Washington University, USA
Andrew Granville	Université Montréal, Canada	Richard Rebarber	University of Nebraska, USA
Jerrold Griggs	University of South Carolina, USA	Robert W. Robinson	University of Georgia, USA
Sat Gupta	U of North Carolina, Greensboro, USA	Filip Saidak	U of North Carolina, Greensboro, USA
Jim Haglund	University of Pennsylvania, USA	James A. Sellers	Penn State University, USA
Johnny Henderson	Baylor University, USA	Andrew J. Sterge	Honorary Editor
Jim Hoste	Pitzer College, USA	Ann Trenk	Wellesley College, USA
Natalia Hritonenko	Prairie View A&M University, USA	Ravi Vakil	Stanford University, USA
Glenn H. Hurlbert	Arizona State University,USA	Antonia Vecchio	Consiglio Nazionale delle Ricerche, Italy
Charles R. Johnson	College of William and Mary, USA	Ram U. Verma	University of Toledo, USA
K. B. Kulasekera	Clemson University, USA	John C. Wierman	Johns Hopkins University, USA
Gerry Ladas	University of Rhode Island, USA	Michael E. Zieve	University of Michigan, USA

PRODUCTION

Silvio Levy, Scientific Editor

Cover: Alex Scorpan

See inside back cover or msp.org/involve for submission instructions. The subscription price for 2017 is US $175/year for the electronic version, and $235/year (+$35, if shipping outside the US) for print and electronic. Subscriptions, requests for back issues from the last three years and changes of subscribers address should be sent to MSP.

Involve (ISSN 1944-4184 electronic, 1944-4176 printed) at Mathematical Sciences Publishers, 798 Evans Hall #3840, c/o University of California, Berkeley, CA 94720-3840, is published continuously online. Periodical rate postage paid at Berkeley, CA 94704, and additional mailing offices.

Involve peer review and production are managed by EditFlow® from Mathematical Sciences Publishers.

PUBLISHED BY

mathematical sciences publishers

nonprofit scientific publishing

http://msp.org/

© 2017 Mathematical Sciences Publishers

involve
2017 vol. 10 no. 4

New algorithms for modular inversion and representation by the form $x^2+3xy+y^2$ 541
Christina Doran, Shen Lu and Barry R. Smith

New approximations for the area of the Mandelbrot set 555
Daniel Bittner, Long Cheong, Dante Gates and Hieu D. Nguyen

Bases for the global Weyl modules of $\mathfrak{sl}_n$ of highest weight $m\omega_1$ 573
Samuel Chamberlin and Amanda Croan

Leverage centrality of knight's graphs and Cartesian products of regular graphs and path powers 583
Roger Vargas, Jr., Abigail Waldron, Anika Sharma, Rigoberto Flórez and Darren A. Narayan

Equivalence classes of $\mathrm{GL}(p,\mathbb{C})\times\mathrm{GL}(q,\mathbb{C})$ orbits in the flag variety of $\mathfrak{gl}(p+q,\mathbb{C})$ 593
Leticia Barchini and Nina Williams

Global sensitivity analysis in a mathematical model of the renal insterstitium 625
Mariel Bedell, Claire Yilin Lin, Emmie Román-Meléndez and Ioannis Sgouralis

Sums of squares in quaternion rings 651
Anna Cooke, Spencer Hamblen and Sam Whitfield

On the structure of symmetric spaces of semidihedral groups 665
Jennifer Schaefer and Kathryn Schlechtweg

Spectrum of the Laplacian on graphs of radial functions 677
Rodrigo Matos and Fabio Montenegro

A generalization of Eulerian numbers via rook placements 691
Esther Banaian, Steve Butler, Christopher Cox, Jeffrey Davis, Jacob Landgraf and Scarlitte Ponce

The H-linked degree-sum parameter for special graph families 707
Lydia East Kenney and Jeffrey Scott Powell